Supramolecular Chemistry
Publication details, including instructions for authors and subscription information:
http://www.informaworld.com/smpp/title~content=t713649759

Self-assembling β-Sheet Tape Forming Peptides

R. P. W. Davies[a]; A. Aggeli[a]; A. J. Beevers[a]; N. Boden[a]; L. M. Carrick[a]; C. W. G. Fishwick[a]; T. C. B. Mcleish[b]; I. Nyrkova[b]; A. N. Semenov[b]
[a] Centre for Self-Organising Molecular Systems, Department of Chemistry, The University of Leeds, Leeds, UK [b] Department of Physics, The University of Leeds, Leeds, UK

To cite this Article Davies, R. P. W. , Aggeli, A. , Beevers, A. J. , Boden, N. , Carrick, L. M. , Fishwick, C. W. G. , Mcleish, T. C. B. , Nyrkova, I. and Semenov, A. N.(2006) 'Self-assembling β-Sheet Tape Forming Peptides', Supramolecular Chemistry, 18: 5, 435 — 443
To link to this Article: DOI: 10.1080/10610270600665855
URL: http://dx.doi.org/10.1080/10610270600665855

Supramolecular Chemistry, July–August 2006 Vol. 18 (5), pp. 435–443

Self-assembling β-Sheet Tape Forming Peptides

R.P.W. DAVIES[a], A. AGGELI[a,*], A.J. BEEVERS[a,†], N. BODEN[a], L.M. CARRICK[a], C.W.G. FISHWICK[a], T.C.B. McLEISH[b], I. NYRKOVA[b,‡] and A.N. SEMENOV[b,‡]

[a]*Centre for Self-Organising Molecular Systems, Department of Chemistry, The University of Leeds, Leeds LS2 9JT, UK;* [b]*Department of Physics, The University of Leeds, Leeds LS2 9JT, UK*

(Received 5 December 2005; Accepted 1 March 2006)

Biological proteins have intrinsically the ability to self-assemble, and this has been implicated in pathological situations called amyloid diseases. Conversely understanding protein self-assembly and how to control it can open up the route to new nanodevices and nanostructured materials for a wide range of applications in medicine, chemical industry and nanotechnology. Biological peptides and proteins have complex chemical structure and conformation. This makes it difficult to decipher the fundamental principles that drive their self-assembling behaviours. Here we review our work on the self-assembly of simple *de novo* peptides in solution. These peptides are designed so that: (i) the chemical complexity of the primary structure and (ii) the conformational complexity are both kept to a minimum. Each peptide adopts an extended β-strand conformation in solution and these β-strands self-assemble in one dimension to form elongated tapes as well as higher order aggregates with pure antiparallel β-sheet structure, without the presence of any other conformations such as turns, loops, α-helices or random coils. Experimental data of the self-assembling properties are fitted with an appropriate theoretical model to build a quantitative relationship between peptide primary structure and self-assembly. These simple systems provide us with the opportunity to reveal the generic properties of the pure β-sheet structures and expose the underlying physicochemical principles that drive the self-assembling behaviour of this biological motif.

Keywords: Molecular self-assembly; Peptides; β-Sheet; Tapes; Fibrils

HIERARCHICAL PEPTIDE SELF-ASSEMBLY

Molecular self-assembly has been attracting increasing interest from the scientific community in the recent years due to its importance in understanding biology and a variety of diseases at the molecular level, and also due to the wide range of potential applications of self-assembled nanostructures in nanotechnology. One-dimensional self-assembly is characterised by aggregate growth only in one dimension, whilst the other dimensions remain constant. Irrespective of the exact chemical nature of the molecular building blocks, most one-dimensional self-assembling systems are governed by similar physicochemical principles, and therefore there are a few common main mechanisms that can describe molecular self-assembly of most systems, such as non-nucleated and nucleated mechanisms. An indication regarding the type of mechanism that underpins self-assembly of one particular system can be obtained by constructing a self-assembling curve, which is the fraction of molecules in aggregates as a function of increasing concentration in solution.

Self-assembly is an intrinsic property of peptide molecules due to their common peptide backbone. Learning to control precisely peptide self-assembly can be a powerful way of constructing a wealth of nanostructured materials and devices with programmable combination of functionalities appropriate for specific applications. However biological peptides and protein molecules are complex systems in terms of their molecular structure (complicated and usually long sequence of amino acid residues), as well as in terms of their folding and self-assembling properties (each protein may consist of a mixture of α-helices, β-sheets, turns, loops and flexible random coil segments). For this reason biological peptides and proteins are not always ideal model systems to expose the fundamental physical and chemical principles that govern protein self-assembly. We have exploited the biological β-sheet motif to design simple *de novo* peptides that self-assemble in one-dimension in a

*Corresponding author . E-mail: a.aggeli@leeds.ac.uk
†Current address: Department of Biological Sciences, University of Warwick, Coventry, CV4 7AL, UK.
‡Current address: Institut Charles Sadron, 6 rue Bossingault, 67083 Strasbourg Cedex, France.

ISSN 1061-0278 print/ISSN 1029-0478 online © 2006 Taylor & Francis
DOI: 10.1080/10610270600665855

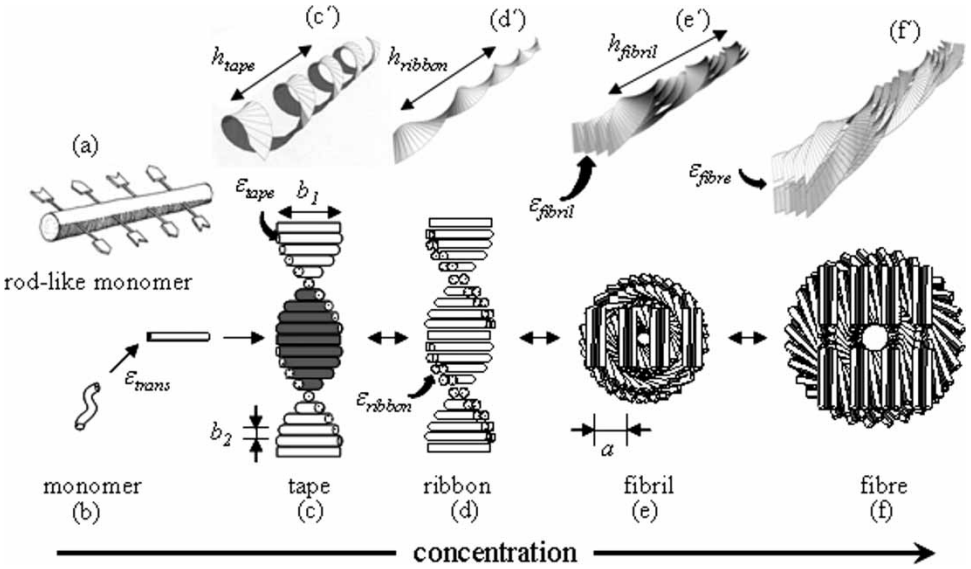

FIGURE 1 Model of hierarchical self-assembly of chiral rod-like units. Local arrangements (c–f) and the corresponding global equilibrium conformations (c′–f′) for the hierarchical self-assembling structures formed in solutions of chiral molecules (a), which have complementary donor and acceptor groups, shown by arrows, via which they interact and align to form tapes (c). The black and white surfaces of the rod (a) are reflected in the sides of the helical tape (c), which is chosen to curl toward the black side (c′). The outer sides of the twisted ribbon (d), of the fibril (e), and of the fibre (f) are all white. One of the fibrils in the fibre (f′) is drawn with darker shade for clarity. (e and f) The front views of the edges of the fibrils and fibres, respectively. Geometrical sizes (the numbers in parentheses show the values of the corresponding geometric sizes for P_{11}-1 and P_{11}-2 peptides, based on x-ray diffraction data and molecular modeling) interrod separation in a tape b_2 ($b_2 = 0.47$ nm); tape width, equal to the length of the rod, b_1 ($b_1 = 4$ nm); inter ribbon distance in the fibril, α ($\alpha = 1.6–2$ nm for P_{11}-1, and $\alpha = 2–2.4$ nm for P_{11}-2) [3].

hierarchical manner to form a variety of well-defined twisted μm-long nanostructures such as tapes (single molecule in thickness), ribbons (a pair of stacked tapes back to back), fibrils (a bundle of stacked ribbons) and fibres (a pair of fibrils interacting edge-to-edge) (Fig. 1) [1–3]. This hierarchical β-sheet self-assembly of peptides follows the 'nucleated one dimensional self-assembly mechanism'. A theoretical model has been developed to rationalise this self-assembly process in terms of five molecular energetic parameters (ε_{trans}, ε_{tape}, ε_{ribbon}, ε_{fibril}, ε_{fibre} all in units of k_bT) and two elastic energies (bend and twist) [4,5]. The magnitudes of these parameters will dictate the self-assembling curve, the critical concentration C^* for the start of self-assembly, length, morphology, stability and dynamic behaviour of the peptide aggregates in solution. This model is summarised below.

Monomeric peptides initially exist in an unordered confirmation in very dilute solutions, where the ϕ and ψ angles of the peptide backbone have any values (Fig. 1b). For peptides to self-assemble in the one-dimension they must undergo a conformation transition, associated with the straightening out of the peptide chain. This process is described by the energetic parameter $\varepsilon_{trans}k_bT$ (free energy change per molecule), and is mainly entropic in nature (Fig. 1b). One dimensional self-assembly continues when there are positive bonding interactions between peptide monomers. This process is quantified by the term $\varepsilon_{tape}k_bT$ (the free energy change due to the association of two peptides) which is mainly enthalpic in nature (Fig. 1c). Indeed self-assembly of antiparallel β-sheet tapes starts at high enough concentration (C^*_{tape}), and only occurs when the loss of entropy is counterbalanced by the gain in enthalpy (Fig. 1c). The critical tape concentration (C^*_{tape}) is related to the energetic parameters involved by the following expression:

$$C^* = \left(\frac{1}{\upsilon_\beta}\right)\exp(\varepsilon_{trans} - \varepsilon_{tape}) \qquad (1)$$

where υ_β is the effective volume of chemical bonds (per peptide) between the peptides in a tape, ε_{trans} is the magnitude of (Table I) conformational energy and ε_{tape} corresponds to the magnitude of scission energy of tapes (association energy).

It is the magnitudes of ε_{trans} and ε_{tape} that govern the position of C^*_{tape}, a low ε_{trans} corresponds to a low C^*_{tape}, whilst a low ε_{tape} corresponds to a high C^*_{tape}.

The number average aggregate size of tapes (M_n) at each concentration (C) is also governed by the magnitude of ε_{tape}:

$$M_n = \left[\upsilon_\beta(C - C^*)\exp\left(\varepsilon_{tape}\right)\right]^{0.5} \qquad (2)$$

And the mean tape length (L_n) is given by:

$$L_n = M_n^* 0.47\,\text{nm} \qquad (3)$$

Tapes are the simplest of the hierarchical structures. A tape at equilibrium is not flat (Fig. 2),

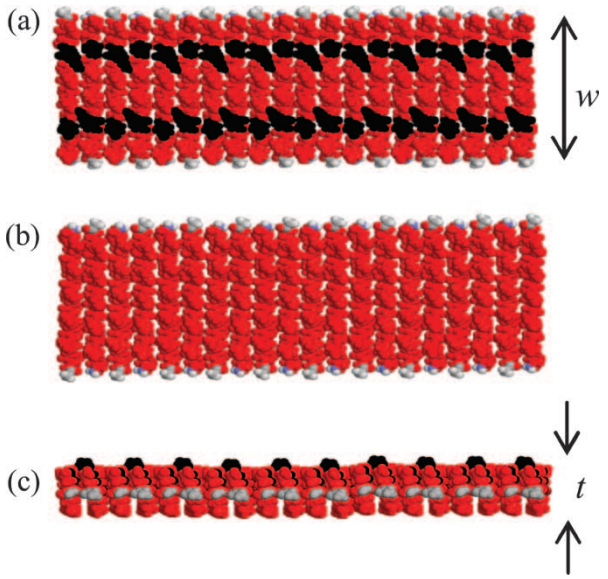

FIGURE 2 Space filling model of P_{11}-1 (Table I) tape. Charged side-chains are black, other polar side chains are coloured red [3].

but helical (Fig. 3a) [6,7]; this is the result of the simultaneous tape twist (due to the chirality of the peptides) and bend (due to the difference between the upper and lower sides of the tape). Two tapes can associate to form a ribbon, stabilised by ε_{ribbon} k_bT (Fig. 1d). The magnitude ε_{ribbon} (the free energy change per pair of stacked peptides) is due to the intermolecular side chain-side chain interactions. In the case of amphiphilic tapes in water, the hydrophobic faces will adhere and the hydrophilic faces will be in contact with water thus giving rise

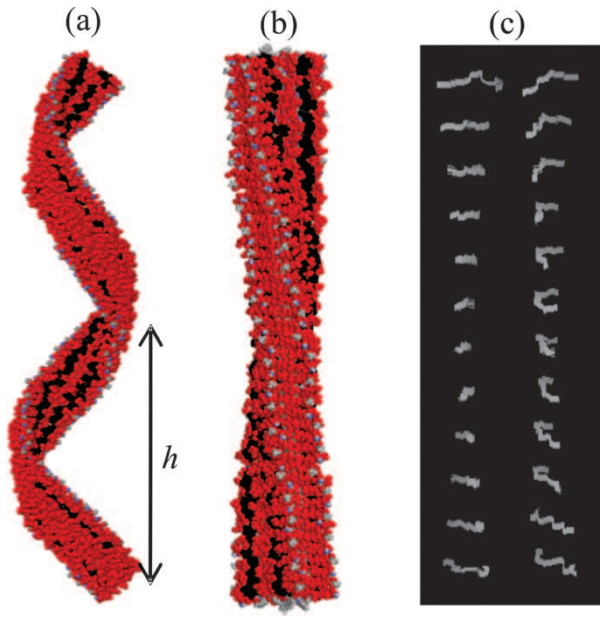

FIGURE 3 Molecular modelling of self-assembled peptide nanostructures. (a) A segment of P_{11}-1 tape with a helical turn (h) viewed from side. (b and c) A segment of P_{11}-2 ribbon [7].

to ε_{ribbon}. Opposing the stacking of two tapes into a ribbon is the elastic energy $\varepsilon^{elast}_{ribbon}$ its origin is due to the helical nature of the tapes. For two tapes to stack together both must decrease their bend and twist to facilitate the presence of one another. The resultant ribbon has more of a saddle curvature (Fig. 3b) rather than the helical twist that is observed for the tapes (Fig. 3a). Energetically, if ε_{ribbon} compensates $\varepsilon^{elast}_{ribbon}$ this will then allow ribbon formation.

If several ribbons stack one on top of each other they will form a fibril (Fig. 1e). Stabilising this structure is $\varepsilon_{fibril}k_bT$, this is the free energy change per pair of stacked peptides in the fibril. As in the formation of tapes, there is an energy cost that restricts fibril formation; this is in the form of $\varepsilon^{elast}_{fibril}$ this is the elastic penalty associated with the untwisting of the ribbons upon stacking. If ε_{fibril} is greater than $\varepsilon^{elast}_{fibril}$ then the self-assembly of fibrils will occur.

The number of tapes/ribbons stacked in a fibril is determined by a balance between the gain in attraction energy (ε_{fibril}) associated with ribbon stacking and the elastic cost (untwisting) associated with packing the ribbons in the fibril. A ribbon characterised by a large twist angle between adjacent peptides, will have a short twist pitch (h), thus giving rise to a high elastic penalty in untwisting (large $\varepsilon^{elast}_{fibril}$). If this condition is combined with a low to moderate ε_{fibril}, a ribbon (not a fibril) would be the resultant equilibrium structure in solution (Fig. 4, region 1). Conversely a small twist angle will induce a long twist pitch of the ribbon. If this condition is combined with a high ε_{fibril} magnitude (Fig. 4, region 2), there will be complete untwisting of the ribbon, and the formation of an infinite stack or a two dimensional crystal will occur. A third intermediate possible scenario could be ribbons characterised by a low to moderate twist angle which would impart an intermediate to long twist pitch to the ribbon. If this was combined with a low to intermediate ε_{fibril}, it will give rise to distinct fibrils with a well-defined number of stacked ribbons per fibril (Fig. 4, region 3).

Once a stable fibril has formed it is possible that a pair of fibrils can entwine edge-on-edge resulting in the formation of a fibre (Fig. 1f). Fibre formation occurs due to the mutual attraction of the C and N termini on the ends of each peptide pair. Fibres are stabilised by $\varepsilon_{fiber}k_bT$, which is the free energy change per pair of associating peptides on two different fibrils. The detailed structures of the peptide aggregates have been confirmed by a wide range of complimentary techniques including CD–UV [3], FTIR [1,2], and fluorescence [8] spectroscopies, transmission electron [2,3] and atomic forces microscopies [9], computer molecular modelling [6], as well as X-ray and electron diffraction data (unpublished results).

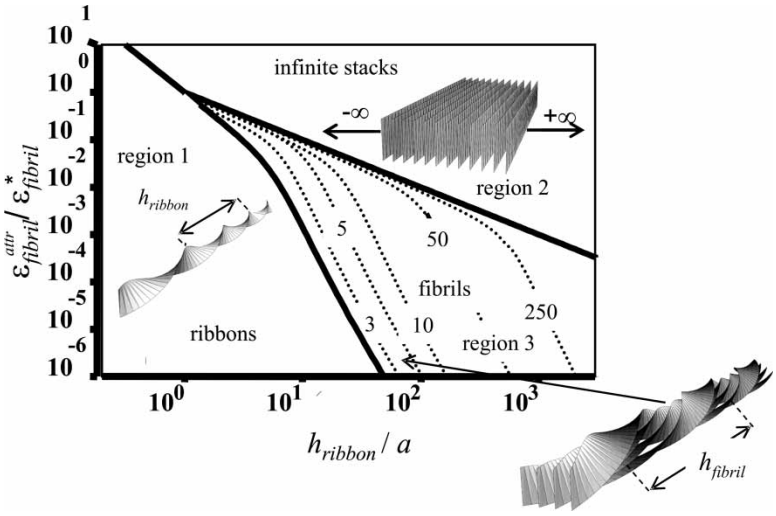

FIGURE 4 Phase diagram of a solution of twisted ribbons that form fibrils. The scaled variables are as follows: relative helix pitch of isolated ribbons h_{ribbon}/α and relative side-by-side attraction energy between ribbons $\varepsilon^{\text{attr}}_{\text{fibril}}/\varepsilon^{*}_{\text{fibril}}$ The areas divided by the thick lines reveal the conditions where ribbons, fibrils and infinite stacks of completely untwisted ribbons are stable. The dotted lines are lines of stability for fibrils containing p ribbons [3].

In summary if: $\varepsilon_{\text{trans}} > \varepsilon_{\text{tape}} > \varepsilon_{\text{ribbon}} > \varepsilon_{\text{fibril}} > \varepsilon_{\text{fibre}}$ then the critical concentrations necessary for the corresponding aggregates to form is in the order $C^*_{\text{tape}} < C^*_{\text{ribbon}} < C^*_{\text{fibril}} < C^*_{\text{fibre}}$. We note that, although this is indeed the generic order of formation, as driven by a "normal" ordering of the attractive energy scales, other orders are possible. For example, charged groups on the peptide termini may give rise to especially strong edge-to-edge attractions of the tapes, so re-ordering $\varepsilon_{\text{fibril}}$ and $\varepsilon_{\text{ribbon}}$ in the series above. In this case the first composite assembly beyond the tape would be a hollow faceted tube. Such structures have indeed been observed [10]. As well as providing such a framework of qualitative classification for self-assembled structures, a further advantage of having a reliable theoretical framework is that by fitting the experimentally derived self-assembling curves with the theoretical model, we can start establishing a quantitative relationship between molecular structure and solution conditions with magnitudes of the energetic parameters. For example the number average aggregate size of tapes (M_n) and critical concentration (C^*_{tape}) can be obtained by experiment and then by using Eq. (2) the magnitude of the energetic parameter $\varepsilon_{\text{tape}}$ can be estimated. By using this value and by applying Eq. (1) the peptide conformational energy $\varepsilon_{\text{trans}}$ will also be known. To demonstrate the way this method would work in practice, we cite the following example:

The peptide P_{11}-2 (Table I) has been rationally designed to undergo the hierarchical process in Fig. 1 [3]. Each amino acid has been positioned according to a number of design principals. Firstly this peptide was based on the polar glutamine forming strong intermolecular hydrogen bonding interactions (polar zippers) to increase the β-tape stability. Alternating polar/apolar side chains were placed in the middle of the peptide; this was done to maximise the potential for β-strand formation and to align the peptides with respect to each other. Hydrophobic tryptophan and phenylalanine have a propensity for $\pi-\pi$ stacking and were placed on the same side of the β-sheet in order to drive one dimensional tape self-assembly. Finally glutamic acid and arginine were included towards either end of the peptide to drive one dimensional tape self-assembly and to stabilise the anti parallel β-sheet state. The N and C termini were blocked to avoid edge-to-edge coulombic interactions. By employing circular dichroism UV spectroscopy (Fig. 5a) and transmission electron microscopy, the self-assembling curve (Fig. 5b), as well as the length and morphologies of the peptide aggregates were obtained (Fig. 5c and d). Fitting of the experimental data with the theoretical model has provided estimates of the magnitudes of the energetic parameters driving self-assembly (Fig. 5b), such as $\varepsilon_{\text{trans}} = 3\,k_bT$, $\varepsilon_{\text{tape}} = 24.5\,k_bT$, and $\varepsilon_{\text{ribbon}} = 0.6\,k_bT$ [3]. The scission energy of a fibril made of eight stacked tapes (energy required to break the fibril into two segments) is equal to $8 \times \varepsilon_{\text{tape}}$, which is estimated to be $\sim 200\,k_bT$. This is similar in magnitude to the scission energy of a covalent bond, which demonstrates the remarkable strength and stability of the peptide aggregates.

Another application, currently under development, of the coarse-grained model of aggregation is its use in establishing a connection to fully-atomistic simulation. It is well beyond the capabilities of current computing power to predict the structure and appearance of the large self-assembled

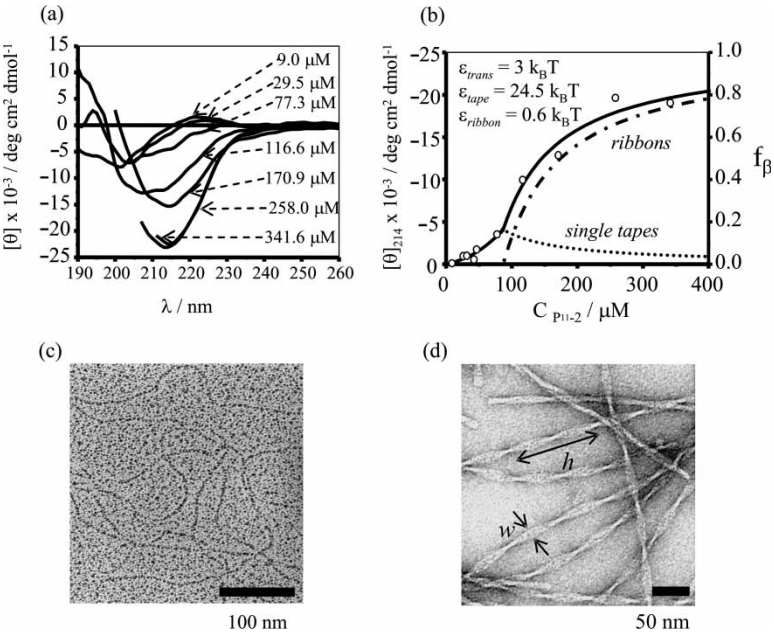

FIGURE 5 Self-assembly of P_{11}-2. (a) Far-UV–CD spectra in water at 20°C. The negative ellipticity at *ca*. 200 nm and a positive ellipticity at *ca*. 222 nm in spectra for $c < 50$ μM is characteristic of random coil monomeric peptide, whereas the negative CD band at *ca*. 214 nm and the positive band below *ca*. 195 nm, at 150 μM $<$ *ca*. $<$ 400 μM is typical of a β-sheet conformation. (b) Fit of the theoretical model (solid line) for the self-assembly of peptides into single and double β-sheet tapes, to the measured concentration dependence of the mean residue ellipticity [θ] of the negative CD band at $\lambda = 214$ nm. $[\theta]_{214}$ is taken to be a linear function of the fraction f_β of peptides in β-sheet tapes. The fractions of peptides involved in single and double tapes are represented with dotted and dash-dot lines, respectively. Negatively stained TEM images of P_{11}-2 forming (c) ribbons and (d) twisted fibrils, formed after prolonged storage of solutions containing P_{11}-2 ribbon [3].

structures using "brute force" simulation. However, the small series of energetic parameters ε_i may be themselves calculated from manageable simulations of a small section of peptide tape [11].

GELATION AND LIQUID CRYSTALLINITY

As the peptide concentration increases so too does the average length and the number of peptide aggregates (Eq. 2). At a certain concentration (C^*_{gel}) the average distance between aggregates becomes shorter than their length, and the aggregates start interacting with each other in space. Solutions with $C < C^*_{gel}$ are said to be in the dilute regime, whilst solutions with $C > C^*_{gel}$ are said to be in the semidilute regime. The more flexible tapes and ribbons, characterised by persistence lengths of tens to hundreds of nm (Fig. 5c) produce random/isotropic topological entanglements (Fig. 6a) in the semi dilute regime, and give rise to a continuous 3-D sponge-like structure which causes gelation of the solution. The more rigid fibrils, characterised by persistence length of μm (Fig. 5d), behave like semi-rigid rods, and above a certain concentration $C^*_{I/N}$ they align into nematic domains, which at higher concentrations, get connected with fibre-like junctions, to give rise to an anisotropic gel structure [12–14]. This causes the solution to undergo a transition from the isotropic to the nematic liquid crystalline state (Fig. 6b) that can be monitored, e.g. by polarised optical microscopy (Fig. 6c).

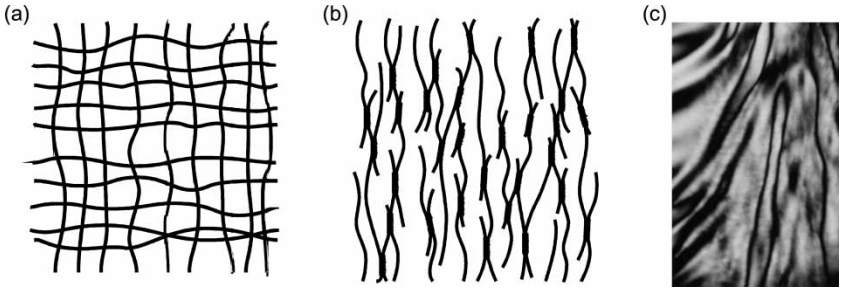

FIGURE 6 Schematic showing global arrangement of an isotropic gel network of semi flexible peptide tapes (a), anisotropic birefringent gel network of inter connected semi rigid peptide fibrils (b) and the thick thread-like texture observed for a nematic solution of P_{11}-2 with $c = 3.7$ mM in a 0.2 mm pathlength microslide, between cross polars (c) [3].

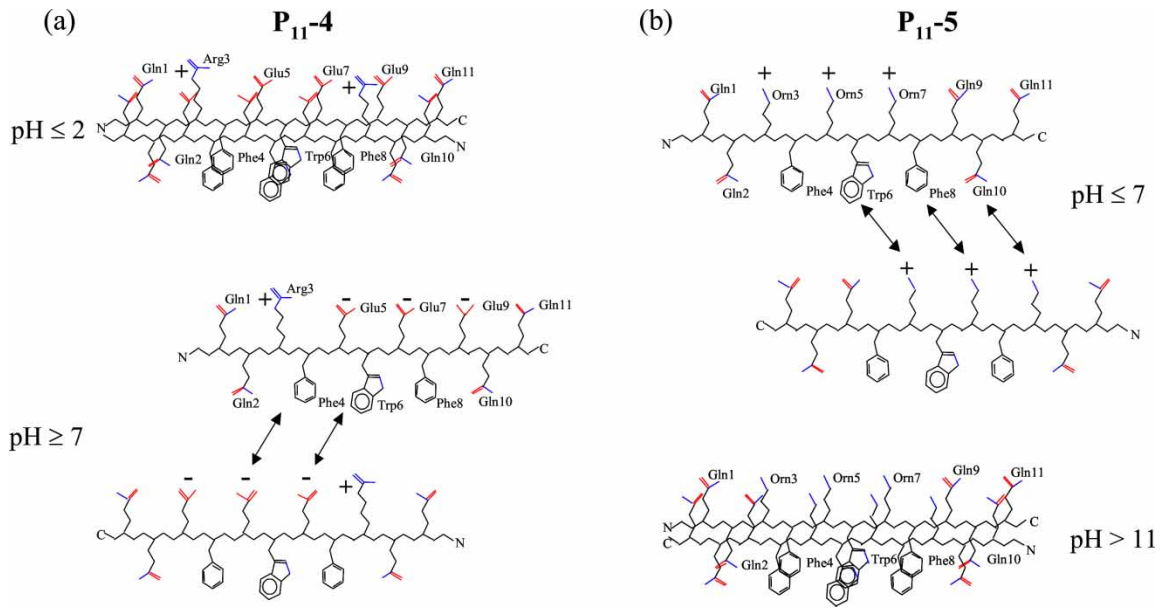

FIGURE 7 Ionization states of P_{11}-4 and P_{11}-5 at low and high pH values showing the side-by-side organisation of peptides in dimeric tape-like substructures and in their dissociated monomeric states [15].

RESPONSIVENESS TO EXTERNAL TRIGGERS

The magnitudes of energetic parameters of the self-assembling peptides are dependant on a number of variables such as solution conditions (pH, ionic strength, relative dielectric constant) and molecular/chemical permutations (peptide length, amino acid composition). Here we describe the effect of pH on peptide self-assembly.

Solutions of P_{11}-2 peptide are stable gels below pH 5, where only arginine is positively charged and the total net charge is +1 per peptide. Above pH 5 the net charge is 0 hence flocculation of the peptide occurs [15]. On the basis of such observations, it becomes apparent that stabilisation of fibrillar dispersions requires of the order of one unit of net positive or negative charge per peptide molecule. Incorporation of further charged groups in the primary structure of P_{11}-2 molecule, such as Glu ($-CH_2CH_2COOH$) or Orn ($-CH_2CH_2CH_2NH_2$), enables self-assembly to be rapidly (seconds) and reversibly controlled by simply changing pH [15].

This is demonstrated by the behavior of two peptide variants: P_{11}-4 (Table I) which can be switched from its nematic to its isotropic fluid state by increasing pH, and P_{11}-5 (Table I) designed to exhibit the converse behaviour (Fig. 7). In these two peptides, the interpeptide association energies, such as ε_{tape}, are strongly influenced by direct electrostatic forces between $\gamma-COO^-$ in Glu^-, or $\delta-NH_3^+$ in Orn^+, respectively. This is illustrated by the acid-base titrations of fibrillar dispersions which reveal deprotonation of the $\gamma-COOH$ of Glu or of the $\delta-NH_3^+$ of Orn^+ occurs over wide bands of up to 5 pH units, a feature of polyelectrolytes. The values of the energy parameters controlling self-assembly and C^*_{tape} values can therefore be smoothly and continuously varied by changing pH. This enables fast isotropic fluid-to-nematic transitions to be triggered by relatively small additions of acid or base, typically 1 part in 10^3 by volume of 1 M HCl or NaOH (Figs. 8 and 9).

HETEROAGGREGATES FORMED BY COMPLEMENTARY PEPTIDES

Another way to change the magnitudes of the energetic parameters and greatly affect the tendency for self-assembly, without changing the solution conditions, is to mix solutions of complementary peptides together. Two such peptides P_{11}-5 (cationic) and P_{11}-4 (anionic) have been previously designed (Fig. 10) [16]. The two complementary peptides must have a propensity to antiparallel β-sheet formation, appropriate complementarity in the disposition of charged amino acid side chains, and at least one additional charged amino acid per peptide pair to stabilise the peptide fibrillar network (Table I).

It has been demonstrated that polyelectrolyte β-sheet complexes (PECs) are formed on mixing aqueous solutions of such cationic and anionic peptides, based on NMR, CD–UV and FTIR spesctroscopic studies (Fig. 11a and b). This results in the spontaneous self-assembly of fibrillar networks (Fig. 11d) and the production of nematic hydrogels (Fig. 11c). These complexes have a 1:1

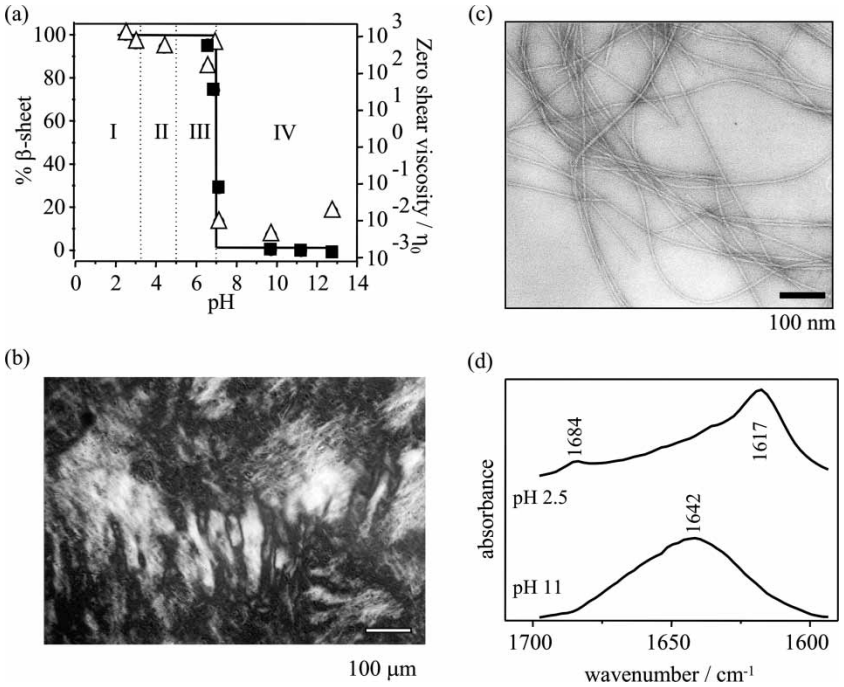

FIGURE 8 (a) Phase behavior of P_{11}-4 at $c = 6.3$ mM, as a function of pH (DCl/NaOD): (I) nematic gel, (II) flocculate, (III) nematic fluid, (IV) isotropic fluid. (■) zero shear viscosity, and (△) % β-sheet determined using FTIR spectroscopy: the continuous line denotes the proportion of peptide in fibrils. (b) Polarizing optical micrograph of a P_{11}-4 gel in water ($c = 6.3$ mM, pH 3) showing a typical thick threadlike viscoelastic nematic texture (path length = 0.2 mm). (c) Transmission electron micrograph of a P_{11}-4 gel in water ($c = 6.3$ mM, pH = 3) showing semirigid fibrils and fibers. (d) FTIR spectrum of amide I′ bands showing β-sheet conformation of P_{11}-4 nematic gel ($c = 6.3$ mM) in DCl at pH 2.5 and random coil state of P_{11}-4 isotropic fluid ($c = 6.3$ mM) in NaOD at pH 11 [15].

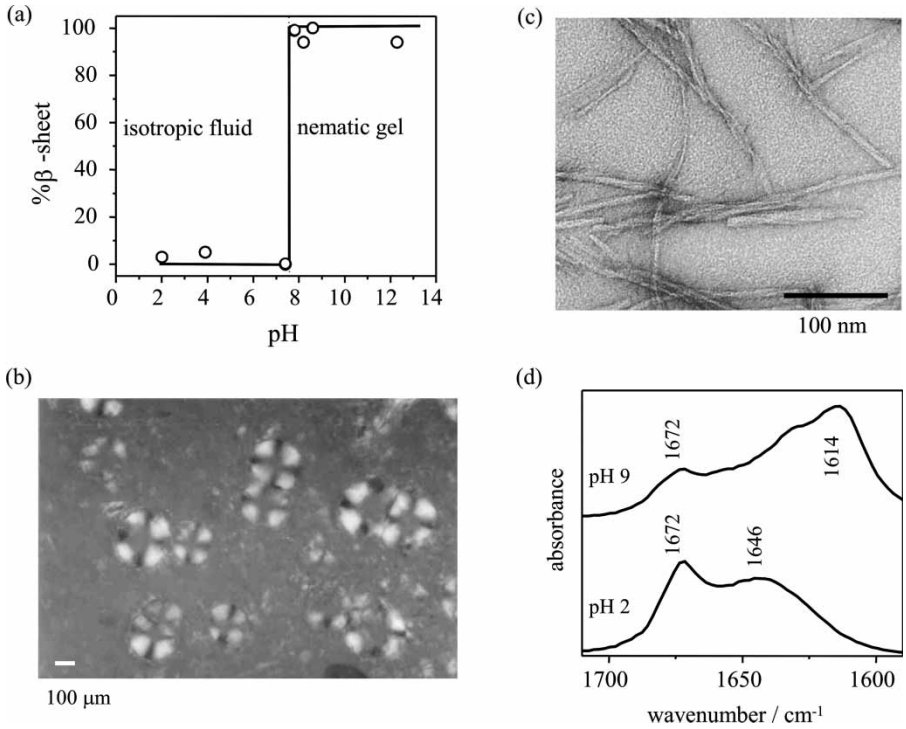

FIGURE 9 (a) Phase behavior of P_{11}-5 ($c = 13.1$ mM in water) as a function of pH (DCl/NaOD), showing the sharp transition from isotropic fluid to nematic gel states at pH 7.5. (b) Polarizing optical micrograph showing nematic droplets with a radial director distribution (maltese cross) dispersed in an isotropic fluid phase. (c) Transmission electron micrograph of a gel (pH 9, $c = 13.1$ mM) showing semirigid fibrils. (d) FTIR spectrum of amide I′ bands showing β-sheet conformation of P_{11}-5 in the nematic gel state ($c = 13.1$ mM, pH 9, NaOD), and the random coil conformation in the isotropic fluid state ($c = 13.1$ mM, pH 2, DCl) [15].

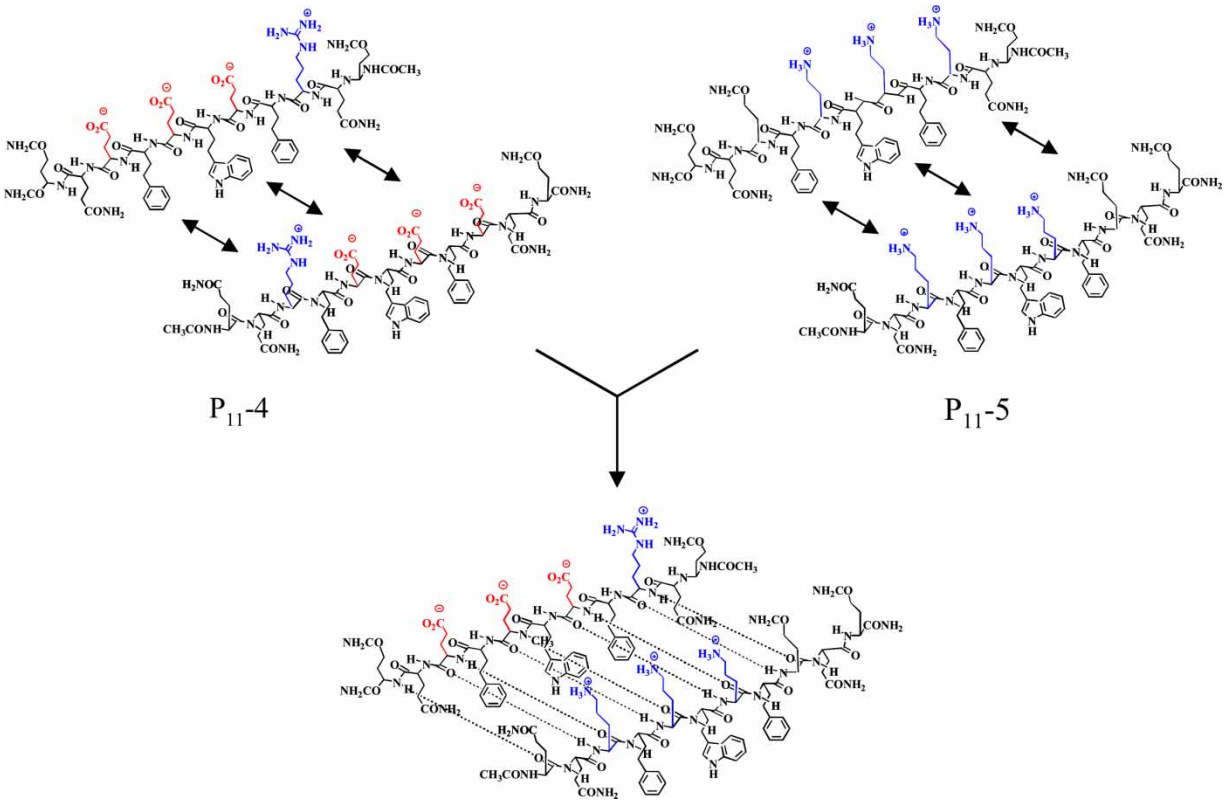

FIGURE 10 Molecular structures of P_{11}-4, P_{11}-5, and the complex showing the electrostatic charge distributions at pH 7.3 [16].

molar stoichiometry and their networks are quite robust to variations in pH or peptide concentration. They may be likened to the PECs formed on mixing oppositely charged polymeric polyelectrolytes except that their supramolecular structures are quite different. In the case of peptide complexes, the fibrils have more definitive molecular and mesoscopic structures making it easier to specify the requisite molecular design.

CONCLUSIONS

Experimental studies of model peptides that form *pure* β-sheet structures, combined with appropriate theoretical models can expose the *generic* properties of the biological β-sheet motif, the fundamental physicochemical principles that govern its formation, and ultimately establish a quantitative link between peptide molecular structure and solution conditions and self-assembling properties that can be used for predictive purposes. It will also further our understanding of the pathological amyloid structures at the molecular level, as well as inspire approaches for their destabilisation in the treatment of amyloid diseases. Although in this paper we have limited ourselves to the summary of the self-assembling properties of pure β-sheet structures in *bulk solution*, another equally important area of research involves the way external fields and structures, such as *solid surfaces* [9] or *lipid layers* [17] can modulate peptide self-assembly and change their equilibrium behaviour. The insight gained can also be used in the growing field of nanotechnology in the precise control of the self-assembling properties of peptide molecular bricks for the production of well-defined, functional nanostructures such as single molecule thick surface coatings [9], templates for nanostructured inorganic materials [18,19], or materials for medical applications [20,21].

TABLE I Peptide primary structures

Peptide	Primary structure	Polymer morphology
P_{11}-1	CH_3CO–Gln–Gln–Arg–Gln–Gln–Gln–Gln–Gln–Glu–Gln–Gln–NH_2	Tapes and ribbons at pH 1–12
P_{11}-2	CH_3CO–Gln–Gln–Arg–Phe–Gln–Trp–Gln–Phe–Glu–Gln–Gln–NH_2	Ribbons and fibrils at pH 1–12
P_{11}-4	CH_3CO–Gln–Gln–Arg–Phe–Glu–Trp–Glu–Phe–Glu–Gln–Gln–NH_2	Fibrils at pH < 7
P_{11}-5	CH_3CO–Gln–Gln–Orn–Phe–Orn–Trp–Orn–Phe–Gln–Gln–Gln–NH_2	Fibrils at pH > 8

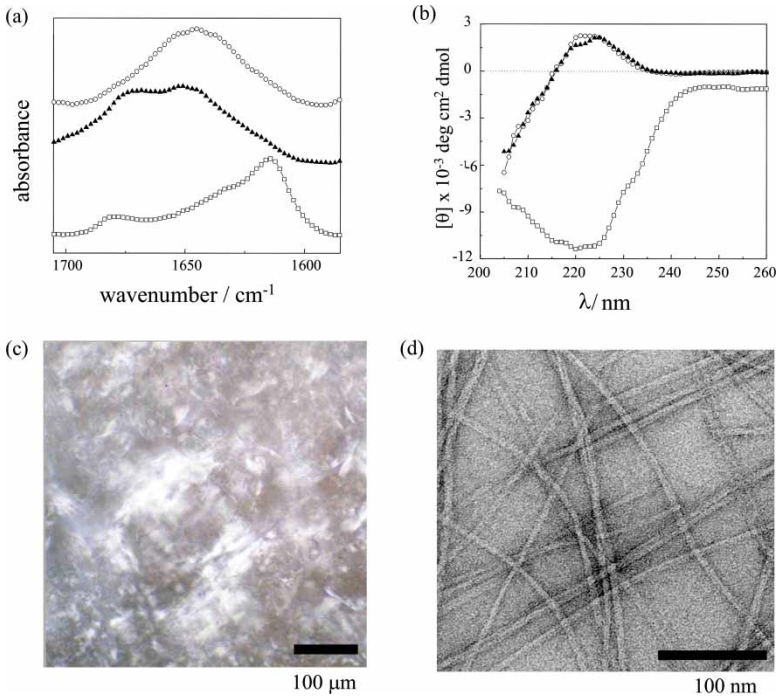

FIGURE 11 (a) FTIR spectra showing amide I′ bands centered at 1645 cm^{-1}, a signature of the initial random coil state of P_{11}-4 (○) and P_{11}-5 (▲) in 6.3 mM aqueous solutions at pH 7.3 prior to mixing, and the β-sheet conformation of the polyelectrolyte complex after mixing (□). (b) Far-UV–CD spectra showing the initial random coil states of P_{11}-4 (○) and P_{11}-5 (▲) in aqueous solutions ($c = 3.1$ mM) prior to mixing, and the β-sheet complex formed after mixing (□). (c) Polarizing optical micrograph of the gel ($c = 6.3$ mm) formed after mixing aqueous solutions of the monomeric peptides at pH 7.3 showing a typical nematic gel texture. (d) Transmission electron micrograph showing mainly fibrils and a few fibers (having twice the diameter of the fibrils) in the nematic gel ($c = 6.3$ mm).

Acknowledgements

The work summarised here has been funded by The Royal Society (Royal Society University Research Fellowship to AA) and The Engineering and Physical Sciences Research Council (EPSRC) of the United Kingdom.

References

[1] Aggeli, A.; Bell, M.; Boden, N.; Keen, J. N.; McLeish, T. C. B.; Nyrkova, I.; Radford, S. E.; Semenov, A. *J. Mater. Chem.* **1997**, *7*, 1135–1145.
[2] Aggeli, A.; Bell, M.; Boden, N.; Keen, J. N.; Knowles, P. F.; McLeish, T. C. B.; Pitkeathly, M.; Radford, S. E. *Nature* **1997**, *386*, 259–262.
[3] Aggeli, A.; Nyrkova, I. A.; Bell, M.; Harding, R.; Carrick, L.; McLeish, T. C. B.; Semenov, A. N.; Boden, N. *Proc. Natl. Acad. Sci. USA* **2001**, *98*, 11857–11862.
[4] Nyrkova, I. A.; Semenov, A. N.; Aggeli, A.; Boden, N. *Eur. Phys. J. B* **2000**, *17*, 481–497.
[5] Nyrkova, I. A.; Semenov, A. N.; Aggeli, A.; Bell, M.; Boden, N.; McLeish, T. C. B. *Eur. Phys. J. B* **2000**, *17*, 499–513.
[6] Fishwick, C. W. G.; Beevers, A. J.; Carrick, L. M.; Whitehouse, C. D.; Aggeli, A.; Boden, N. *Nano Lett.* **2003**, *3*, 1475–1479.
[7] Beevers, A. J. Phd Thesis, University of Leeds, **2003**.
[8] Kayser, V.; Turton, D. A.; Aggeli, A.; Beevers, A.; Reid, G. D.; Beddard, G. S. *J. Am. Chem. Soc.* **2004**, *126*, 336–343.
[9] Whitehouse, C.; Fang, J. Y.; Aggeli, A.; Bell, M.; Brydson, R.; Fishwick, C. W. G.; Henderson, J. R.; Knobler, C. M.; Owens, R. W.; Thomson, N. H.; Smith, D. A.; Boden, N. *Angew. Chem. Int. Ed.* **2005**, *44*, 1965–1968.
[10] Jimenez, J. L.; Guijarro, J. L.; Orlova, E.; Zurdo, J.; Dobson, C. M.; Sunde, M.; Saibil, H. R. *Embo J.* **1999**, *18*, 815–821.
[11] Harris, S. A.; Sands, Z. A.; Laughton, C. A. *Biophys. J.* **2005**, *88*, 1684–1691.
[12] Aggeli, A.; Fytas, G.; Vlassopoulos, D.; McLeish, T. C. B.; Mawer, P. J.; Boden, N. *Biomacromolecules* **2001**, *2*, 378–388.
[13] Mawer, P. J.; Waigh, T. A.; Harding, R.; McLeish, T. C. B.; King, S. M.; Bell, M.; Boden, N. *Langmuir* **2003**, *19*, 4940–4949.
[14] Carrick, L.; Tassieri, M.; Waigh, T. A.; Aggeli, A.; Boden, N.; Bell, C.; Fisher, J.; Ingham, E.; Evans, R. M. L. *Langmuir* **2005**, *21*, 3733–3737.
[15] Aggeli, A.; Bell, M.; Carrick, L. M.; Fishwick, C. W. G.; Harding, R.; Mawer, P. J.; Radford, S. E.; Strong, A. E.; Boden, N. *J. Am. Chem. Soc.* **2003**, *125*, 9619–9628.
[16] Aggeli, A.; Bell, M.; Boden, N.; Carrick, L. M.; Strong, A. E. *Angew. Chem. Int. Ed.* **2003**, *42*, 5603–5606.
[17] Protopapa, E.; Aggeli, A.; Boden, N.; Knowles, P. F.; Salay, L. C.; Nelson, A. *J. Med. Phys. Eng.* **2006**, In press.
[18] Meegan, J. E.; Aggeli, A.; Boden, N.; Brydson, R.; Brown, A. P.; Carrick, L.; Brough, A. R.; Hussain, A.; Ansell, R. J. *Adv. Funct. Mater.* **2004**, *14*, 31–37.
[19] Reches, M.; Gazit, E. *Science* **2003**, *300*, 625–627.
[20] Bell, C. J.; Carrick, L.; Katta, J.; Ingham, E.; Aggeli, A.; Boden, N.; Waigh, T. A.; Fisher, J.;, **2006**, In press.
[21] Zhang, S. G.; Gelain, F.; Zhao, X. J. *Semin. Cancer Biol.* **2005**, *15*, 413–420.